iScience

Article

Single-cell RNA sequencing highlights a significant retinal Müller glial population in dry age-related macular degeneration

Graphical abstract

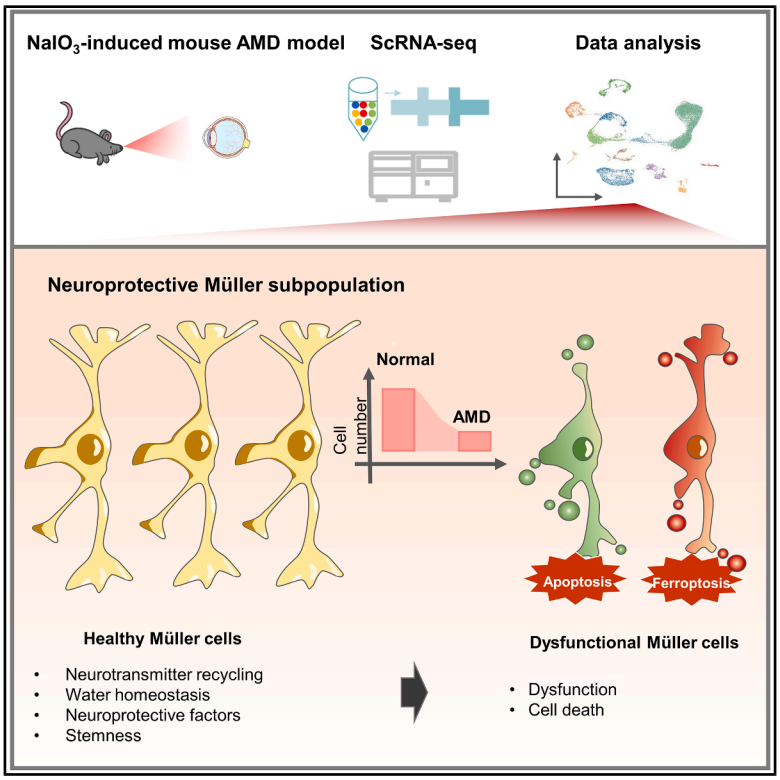

Highlights

- A comprehensive landscape of the $NaIO_3$ model was constructed at the single-cell level
- $Sox2^+$ Müller cells, with a neuroprotective role, were identified
- Ferroptosis and apoptosis significantly reduce $Sox2^+$ Müller cluster in $NaIO_3$ model
- The death of $Sox2^+$ Müller cells is associated with the progression of AMD

Authors

Bing Zeng, Chuanhe Zhang, Yifan Liang, ..., Chang Zou, Dongcheng Liu, Bo Qin

Correspondence

zouchang@cuhk.edu.cn (C.Z.), ldc2025@163.com (D.L.), qinbozf@163.com (B.Q.)

In brief

Pathophysiology; Complex system biology; Transcriptomics

Zeng et al., 2025, iScience 28, 112464
May 16, 2025 © 2025 The Author(s). Published by Elsevier Inc.
https://doi.org/10.1016/j.isci.2025.112464

CellPress

iScience

CellPress
OPEN ACCESS

Article

Single-cell RNA sequencing highlights a significant retinal Müller glial population in dry age-related macular degeneration

Bing Zeng,[1,2,3,8] Chuanhe Zhang,[1,2,8] Yifan Liang,[1,2] Jianguo Huang,[1,2] Deshuang Li,[1,2] Ziling Liu,[1,2] Hongxia Liao,[1,2] Tedu Yang,[4] Muyun Liu,[5] Chang Zou,[6,*] Dongcheng Liu,[1,2,7,*] and Bo Qin[1,2,7,9,*]

[1]Shenzhen Aier Eye Hospital, Aier Eye Hospital, Jinan University, Shenzhen, China
[2]Shenzhen Aier Ophthalmic Technology Institute, Shenzhen, China
[3]Department of Ophthalmology, Xiangya Hospital, Central South University, Changsha 410008, Hunan, China
[4]Shenzhen Shendong Aier Eye Hospital, Shenzhen, China
[5]National Engineering Research Center of Foundational Technologies for CGT Industry, Shenzhen Kenuo Medical Laboratory, Shenzhen, Guangdong, China
[6]Department of Clinical Medical Research Center, The Second Clinical Medical College of Jinan University, the First Affiliated Hospital of Southern University of Science and Technology, Shenzhen People's Hospital, Shenzhen, Guangdong, P.R. China
[7]Aier School of Ophthalmology, Central South University, Changsha, China
[8]These authors contributed equally
[9]Lead contact
*Correspondence: zouchang@cuhk.edu.cn (C.Z.), ldc2025@163.com (D.L.), qinbozf@163.com (B.Q.)
https://doi.org/10.1016/j.isci.2025.112464

SUMMARY

The main challenge in dissecting the cells and pathways involved in the pathogenesis of age-related macular degeneration (AMD) is the highly heterogeneous and dynamic nature of the retinal microenvironment. This study aimed to describe the comprehensive landscape of the dry AMD (dAMD) model and identify the key cell cluster contributing to dAMD. We identified a subset of Müller cells that express high levels of Sox2, which play crucial roles in homeostasis and neuroprotection in both mouse models of AMD and patients with dAMD. Additionally, the number of $Sox2^+$ Müller cells decreased significantly during the progression of AMD, indicating these cells were damaged and underwent cell death. Interestingly, ferroptosis and apoptosis were identified as contributors to the damage of $Sox2^+$ Müller cells. Our findings are potentially valuable not only for advancing the current understanding of dAMD progression but also for the development of treatment strategies through the protection of Müller cells.

INTRODUCTION

Dry age-related macular degeneration (AMD) is one of the ophthalmic diseases that give rise to blindness among people aged over 55-years-old worldwide.[1,2] The pathogenesis of AMD is complex and involves numerous factors, including chronic inflammation, lipid deposition, and oxidative stress.[3] In addition, due to the heterogeneity of retinal microenvironments, which contain various cell types and cell-cell communications, the mechanism of dysfunction and injury during the progression of AMD has not been fully understood.[4]

Recent advances in single-cell RNA sequencing (scRNA-seq) technology enable high-resolution and in-depth analysis of the transcriptome in samples with significant heterogeneity. Utilizing scRNA-seq technology, previous studies have emphasized the importance of retinal pigment epithelium (RPE) cells in AMD pathogenesis.[4–7] However, to our knowledge, there are limited studies on the heterogeneity of Müller glia. Müller glia are the only cell type that spans all retinal layers and has contact with almost every cell type in the retina.[8] As Müller cells are crucial to the retina, any disturbance to the retinal environment can influence their proper function, which in turn affects the entire retina.[8,9] It has been found that Müller cells participate in the progression of some eye disorders, such as glaucoma, diabetic retinopathy, and proliferative vitreoretinopathy,[10–12] and those studies focused on the pro-inflammatory function of Müller glia in the retina. In the limited literature on AMD, Müller glia with low mitochondrial DNA expression shows proangiogenic function in the early AMD retina.[13] Additionally, Müller glia with *Gfap* expression may play a role in cellular recovery in a fundus camera-delivered light-induced retinal degeneration model.[14] Nonetheless, the precise role of Müller glia in the progression of AMD remains unclear.

In this study, we constructed a comprehensive cell atlas of the retina using a sodium iodate ($NaIO_3$, SI)-induced dry AMD (dAMD) model through scRNA-seq technology.[15–18] Interestingly, in addition to the RPE cell, Müller glia was one of the cell types with the highest AMD signature score among the retinal microenvironment.[19] Importantly, SRY-Box Transcription

This is an open access article under the CC BY-NC-ND license (http://creativecommons.org/licenses/by-nc-nd/4.0/).

Factor 2 (*Sox2*)$^{+}$ Müller cells (Müller subset 2) with potential protective function were identified. However, this subpopulation of Müller cells significantly decreased in the dAMD model. Furthermore, ferroptosis and apoptosis were found to play a key role in the cell death of the protective Müller subset. Our results suggest that Müller glia are closely related to AMD and the *Sox2*$^{+}$ Müller subcluster plays a potential protective role in the retinal microenvironment. Its deficiency is relevant to the risk of AMD.

RESULTS

ScRNA-seq atlas of the retina in a $NaIO_3$-induced AMD model

To investigate the cellular diversity in the retina microenvironment and find the crucial cell type related to AMD, a $NaIO_3$-induced mouse model, a well-known drug-induced model of geographic atrophy (advanced dAMD),[16,17,20,21] was established (Figure S1), and single-cell transcriptome analysis was performed[22] (Figure 1A). After performing quality control of scRNA-seq data, 20,725 qualified cells were obtained. We utilized the canonical markers and revealed 12 distinct clusters from the mouse retina, including RPE, rod cells, cone cells, cone bipolar cells (CBCs), rod bipolar cells (RBCs), amacrine/horizontal cells (AC/HCs), Schwann/retinal ganglion cells (SC/RGCs), pericytes, fibroblasts, endothelial cells, Müller glia, and immune cells[23–29](Figures 1B–1D). The expression levels of five marker genes of these cell clusters are shown in Figure 1E. Among them, there was a dramatic decrease in the number of RPE cells, while the number of immune cells showed a significant increase in the $NaIO_3$-induced group. Endothelial cells and pericytes were the two subpopulations that appeared to decrease. Compared to the negative control (NC) group, AC/HC, CBC, RBC, and rod cells had a slight change in proportion in the $NaIO_3$-treated mice (Figure 1D). Collectively, we constructed an integrative single-cell transcriptional atlas of the $NaIO_3$-induced model and established a cellular profile for further understanding the dynamic retinal microenvironment during retina degeneration.

Cell-type-specific expression of genes associated with AMD in Müller glial cells

A previous genome-wide association study (GWAS) identified important risk loci associated with AMD in human.[30] To investigate which subset of cells is the most associated with the initiation or progression of AMD, we defined an AMD risk score based on these loci and analyzed the gene expression pattern in each cell cluster (Figure 2A). Thirty-one genes remained after the removal of wet AMD risk loci.[30,31] We then scored all cell clusters for their expression of gene signatures representing AMD risk and found that Müller glia was the cell type with the highest score, in terms of both median score (Figure 2B) and the average score (Figure 2C). Among these genes, Apolipoprotein E (*Apoe*) and Transient Receptor Potential Cation Channel Subfamily M Member 3 (*Trpm3*) were primarily enriched in Müller glia (Figure 2D). Taken together, these results imply a significant relationship between Müller cells and AMD.

The number of Müller glia with a potential protective effect decreased dramatically in the $NaIO_3$-induced AMD model

To further assess the important role of Müller glia in dAMD, 930 Müller glia were categorized into six cell subpopulations through cluster analysis (Figures 3A–3C; Table S1). To characterize each Müller cell subpopulation, we performed Gene Ontology (GO) analysis using upregulated differentially expressed genes (DEGs) (Table S2). Since Müller glia is a source of neuroprotective factors to promote neuronal survival from oxidative stress by providing antioxidants,[32] we noticed that genes upregulated in Müller 2 (Figure 3D) cluster were mainly enriched in five important pathways associated with neuroprotection and homeostasis, including regulation of synapse structure or activity, synapse organization, glial cell differentiation, regulation of neurogenesis, and gliogenesis (Figures 3D–3I; Table S3), indicating that Müller 2 is the most important protector for retina in the dAMD model. To further analyze the properties of Müller 2, functional analysis was performed using gene signatures related to Müller glia.[33–35] We discovered that the Müller cluster 2 displays the highest score in several fundamental signal pathways related to neuroprotection and homeostasis, including neurotransmitter recycling, water homeostasis, and neuroprotective factors (Figures 4A–4C; Figure S2). Interestingly, Müller 2 also displayed the highest stemness score (Figure 4D), suggesting that they might be in a ''stem-like'' state and able to differentiate into new neurons. Indeed, Müller 2 expressed high levels of *Sox2*, which is associated with stem cell stemness.[36–38] The high-expression feature genes of those functions are shown in Figures 4E–4I.

The trajectories of Müller glia were constructed in a pseudotime manner (Figure S3). State 1 comprised Müller 1 and Müller 5, state 3 mainly consisted of Müller 2 and Müller 3, and state 2 primarily comprised rest cells (Figure S3A). From node 1, two branches were formed. The differential expression analysis and GO analysis were executed for each branch (Figure S3B). GO analysis of state 3 enriched in gliogenesis and glial cell differentiation, supporting that Müller 2 had critical functions in neuroprotection and retina homeostasis.

We next asked whether Müller cluster 2 is present in the retina of patients with dAMD. scRNA-seq data from AMD patients were collected and analyzed (https://www.ncbi.nlm.nih.gov/geo/query/acc.cgi?acc=GSE203499, only patients with dAMD and control samples were collected). Müller cluster was separated from the retinal cells, and eight subtypes were identified (Figures S4A and S4B). Indeed, using signature score analysis, we found that a subset of Müller cells in humans, hMüller cluster 4, exhibits a high gene signature score defined by the expression of marker genes of Müller 2 (Figures S4C and S4D). Importantly, the number of these cells was also decreased in dAMD patients compared to healthy individuals (Figure S4B), consistent with data from $NaIO_3$-induced models. The genes associated with the retinal protection functions of Müller cluster 2 were validated in human Müller clusters (Figure S4E).

Briefly, we constructed an integrative transcriptional atlas of Müller glia in the dAMD model, describing the genetic changes in Müller glia clusters during dAMD. More importantly, we identified a significant cluster of Müller glia, Müller 2, which

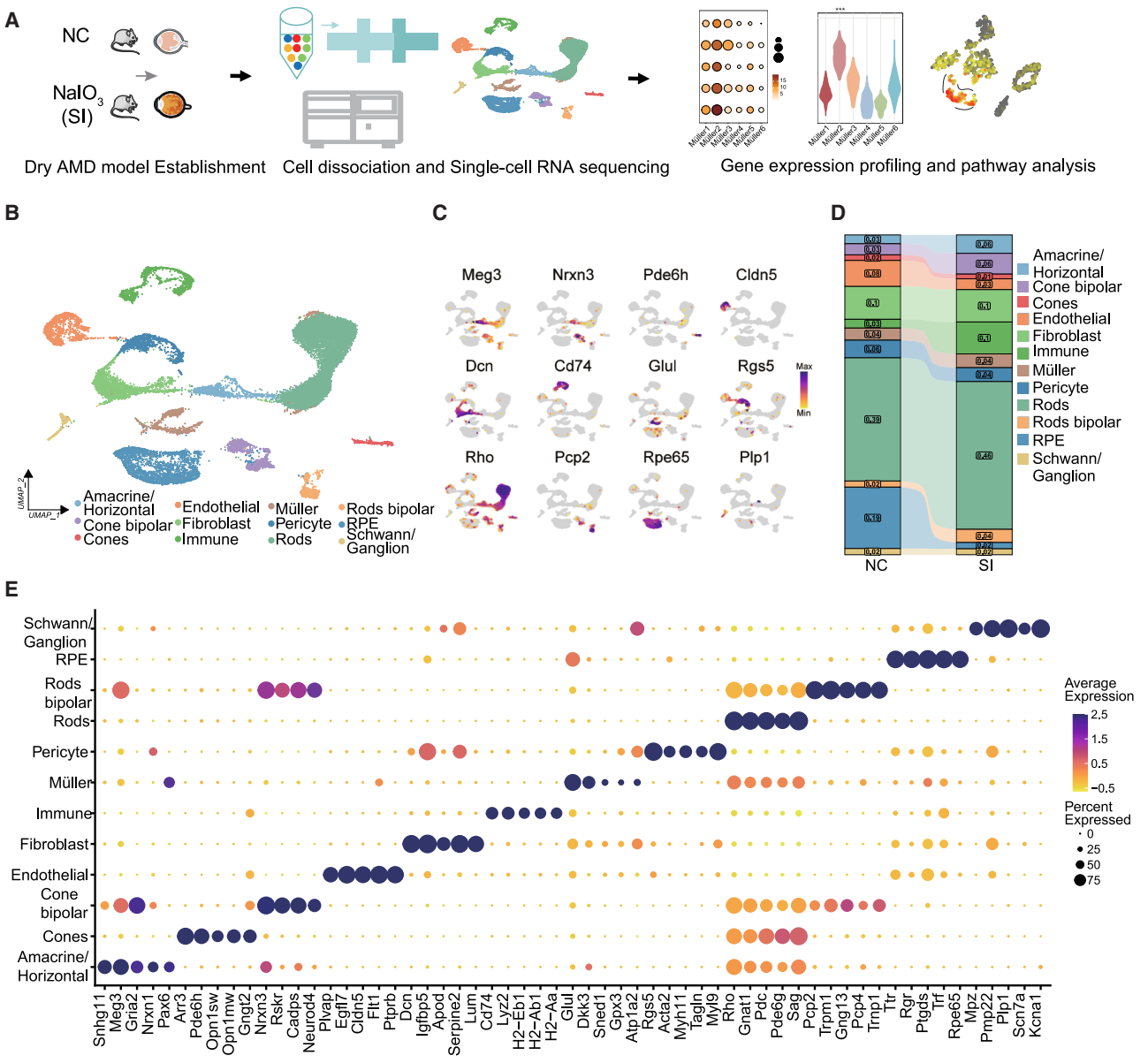

Figure 1. A total of 12 cell types were identified in $NaIO_3$-induced AMD model

(A) The workflow of this study.

(B) The 12 major cell populations were identified in mice.

(C) The UMAP (Uniform Manifold Approximation and Projection) distribution of canonical markers for each cell cluster.

(D) Relative changes in cell ratios among different clusters between the NC and SI ($NaIO_3$) groups.

(E) The average expression level of the top marker genes across 12 clusters.

See also Figure S1.

decreased in both the AMD model and the AMD patient and might play a critical neuroprotective role during AMD progression.

Ferroptosis and apoptosis contribute to cell damage of neuroprotective Müller cell

Given that neuroprotective Müller 2 cells decrease in number during dAMD, we asked which type of cell death was associated with the reduction of Müller 2 cells (Figures 3B and S4B). Through literature and database mining, we collected eight gene sets of pathways associated with cell death and scored Müller cells by their gene expressions. The scores of four cell death-related programs in Müller 2 (including disulfidptosis, autophagy, ferroptosis, and apoptosis) were significantly higher in the $NaIO_3$ group than in the control group (Figure 5A). GO analysis with upregulated DEGs in $NaIO_3$-treated Müller 2 indicated

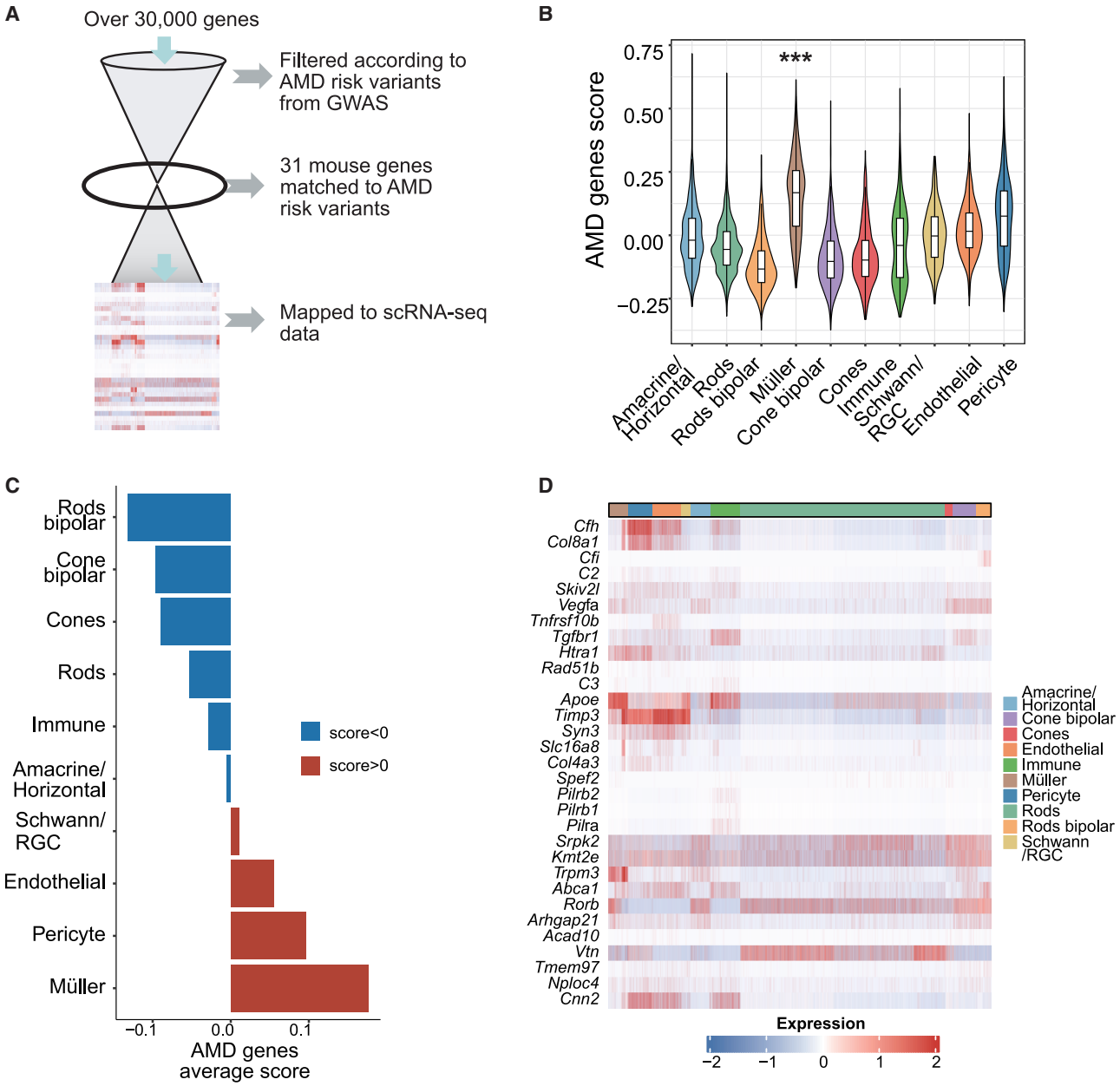

Figure 2. Müller glia are closely related to AMD

(A) The diagram illustrates the strategy for screening AMD risk genes according to specific risk loci of AMD.

(B) The violin plot shows the score of AMD-associated genes in ten retinal cell clusters. The box represents median value.

(C) The boxplot shows the differences in AMD risk scores across various cell types.

(D) The heatmap illustrates the expression levels of 31 AMD-related genes.

*$p < 0.05$, **$p < 0.01$, ***$p < 0.001$, ****$p < 0.0001$, Wilcoxon test.

that this group of Müller cells was related to ferroptosis, iron uptake and transport, and apoptosis (Figures 5B and S5). To further our study, gene set enrichment analysis (GSEA) was performed, and the results showed that ferroptosis and apoptosis were activated in the Müller 2 in the $NaIO_3$ group (Figure 5C). Importantly, a similar result was observed in hMüller cluster 4 in the patient with dAMD (Figure 5D).

Since we are the first to find ferroptosis occurring in Müller cells, to confirm our data, we examined the expression of the critical gene of ferroptosis in Müller 2 by the expression levels of genes (Figures 5E and 5F) and immunofluorescence staining (Figures 5G and 5H). Kelch-like ECH-associated protein 1 (Keap1) is a driver of ferroptosis and regulates ferroptosis in a SLC7A11/GPX4-independent manner in cancer cells.[39] Keap1

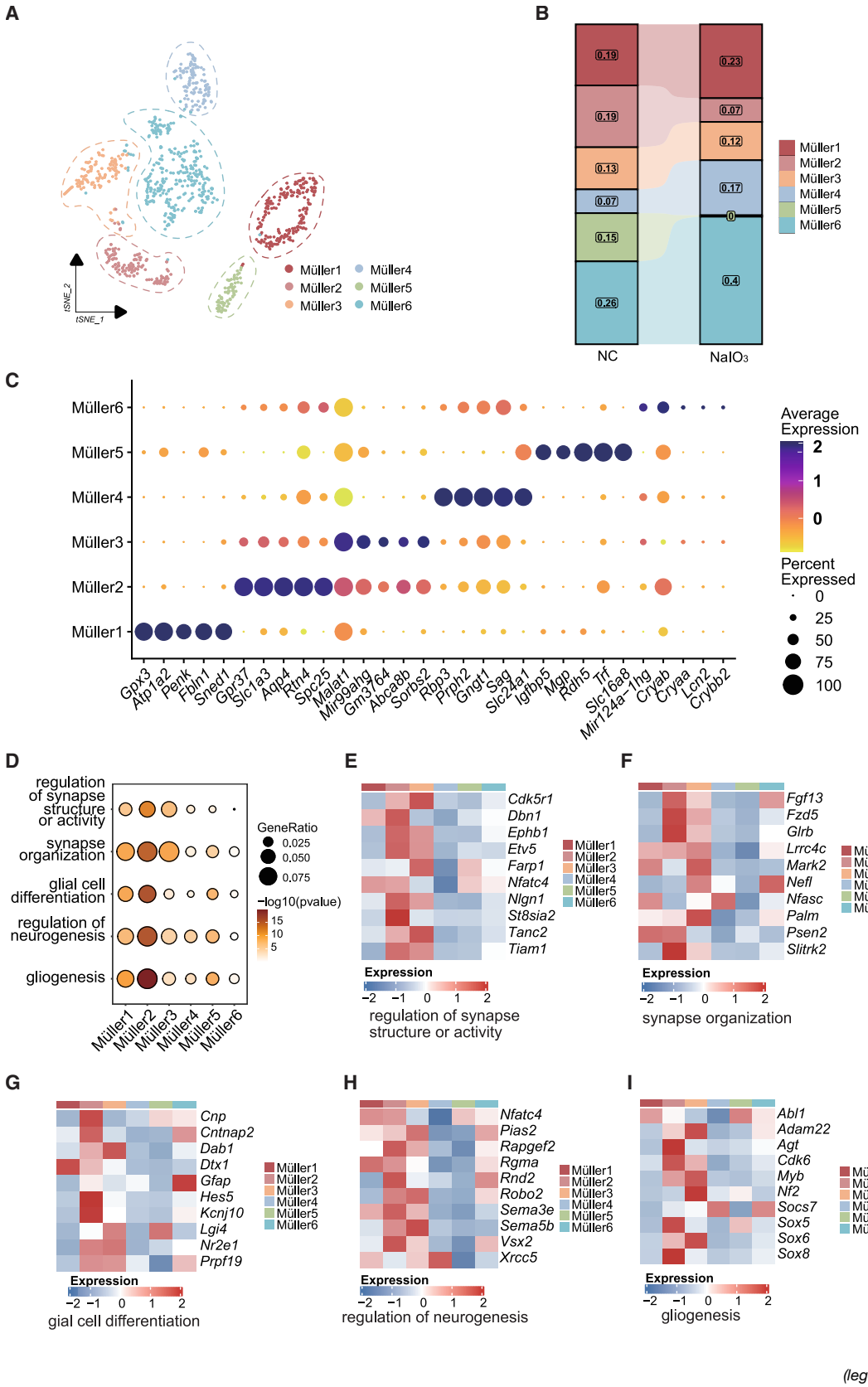

(legend on next page)

was only specifically expressed in Müller 2 in the $NaIO_3$-treated group (Figure 5F). Immunofluorescence results showed that (1) Müller 2 (co-stained with GS and Sox2) was significantly reduced in the dAMD model and (2) ferroptotic Müller 2 (co-stained with GS, Sox2, and Keap1) was markedly increased in the dAMD model (Figures 5G and 5H). Taken together, our results suggested that ferroptosis and apoptosis contributed to the decrease of Müller cells featured with neuroprotection potential in dAMD.

DISCUSSION

In the present study, we revealed the importance of Müller glia in the risk of AMD with $NaIO_3$-induced mouse model, which is consistent with previous findings regarding Müller glia in human AMD.[31] Six subsets of Müller cells were identified. Among them, Müller 2 has a unique gene signature associated with neuroprotective factors, stemness, and neurotransmitter recycling, all of which are essential for retinal metabolism and visual function. Our results suggest that Müller 2 is a potential protector for retinal homeostasis during dAMD development. Furthermore, ferroptosis and apoptosis are the main factors contributing to the reduction of these important Müller cells. Our study also implies that, in addition to apoptosis, ferroptosis may occur in cells other than RPE in the retinal microenvironment during the progression of AMD, particularly in cells with neuroprotective functions.

Müller cells play important functional and regulatory roles in retinal structure, metabolism, and homeostasis.[8] Müller glia is the cell type that reacts first when the retina is injured.[40] Thus, the dysfunction of Müller cells is associated with many retinal diseases, including AMD, macular telangiectasia, and diabetic retinopathy.[19,41,42] A prior study based on the Eye Genotype Expression database found that a series of genes associated with AMD severity are strongly positively correlated with the proportions of Müller glia.[43] In the present study, we found Müller cells showed the highest AMD risk score among retinal cells (RPE cells not included). This result further strengthens the importance of Müller glia in AMD. According to previous research, Müller glia can be activated to produce antioxidants and neurotrophic factors that protect retinal function from further damage.[35] Here, our data showed that Müller cells are highly heterogeneous and that only a portion of them may have properties associated with neuroprotection in the dAMD model. Indeed, some reports show that Müller glia may impair the ability of neurotransmitter removal and dysregulate the ion and water homeostasis in response to pathological conditions, suggesting a detrimental role for Müller glia.[34,44,45] In addition, Müller cells can form glial scars, causing central nervous system failure to regenerate.[34] However, in this study, we found that the Müller 2 subset is a crucial retinal protector that is featured with potential retinal homeostasis and neuroprotection. Indeed, Müller 2 highly expressed Kcnj10 and other important components in the neurotransmitter recycle pathway (Figure 4E). Na^+/K^+ and Ca^{2+} dysregulation have been reported in the pathogenesis of neuronal degenerative diseases.[46] Müller cells can restore physiological pH and ion concentrations by expressing potassium ion channels, Kir4.1, which is encoded by the *KCNJ10* gene, on the plasma membrane. These channels facilitate the movement of K^+ ions from areas of high K^+ concentration to regions with low or stable K^+ concentrations.[47] Interestingly, Müller 2 cells express a multitude of stem cell factors, including Sox2, Sox9, and Nfib, which play important roles in stem cell development and differentiation (Figure 4H). These observations implied that (1) Müller 2 are the main cells that facilitate the formation of new neurons and maintain the viability of photoreceptors and neurons and (2) Müller 2 cells might be in a "stem-like" state, which has the potential to differentiate into new neurons to rebuild the retina and restore vision.[48,49] Therefore, the enhancement and transplantation of this class of cells may represent a novel strategy for the treatment of AMD.

Apoptosis is a classic cell death pathway found in Müller glia in diabetic retinopathy[50,51] and in models of blue light exposure.[52] However, limited studies have reported the observation of apoptosis in Müller during AMD progression. Our study showed that apoptosis contributed to the damage of Müller cells in both the dAMD model and the patient with AMD. Previous research has focused on the damage of RPE and photoreceptors in AMD,[53,54] and our study highlights the important role of cell death in Müller glia, which is featured with potential neuroprotective function in AMD pathogenesis.

Ferroptosis is a newly discovered programmed cell death characterized by lipid peroxidation and iron accumulation.[55] Ferroptosis has been identified in retinal ischemia/reperfusion injury and glaucoma.[56,57] Ferroptosis is the major feature of AMD, with retinal iron accumulation and lipid peroxidation.[58,59] Moreover, the relationship between RPE and ferroptosis has been reported.[15,60–62] By using GSEA, Metascape, and immunofluorescence, ferroptosis is identified and validated in the Müller 2 subpopulation, suggesting that ferroptosis might occur in various cells in the retinal microenvironment during AMD progression. Inhibition of ferroptosis has a protective effect on various types of retinal cells and represents a promising strategy for AMD treatment.

Conclusions

In summary, our study constructed the comprehensive cell landscape, especially the Müller glia atlas, in the $NaIO_3$-induced mouse AMD model. We identified a distinct subpopulation of Müller cells ($Sox2^+$ Müller cells) providing neuroprotection

Figure 3. A distinct subset of Müller glia was identified

(A) The t-SNE (t-distributed Stochastic Neighbor Embedding) distribution of six Müller cell clusters resulted from cluster analysis.

(B) Relative changes in cell ratios in different clusters between NC and SI ($NaIO_3$) groups of Müller cells.

(C) The dot plot shows the mean expression of the preferentially expressed genes in six clusters in Müller cells.

(D) GO enrichment analysis of AMD-upregulated DEGs in six Müller glia clusters of the AMD model.

(E–I) The heatmap plots show the expression of genes in six Müller glia clusters, which are from regulation of synapse structure or activity (E), synapse organization (F), glial cell differentiation (G), regulation of neurogenesis (H), and gliogenesis (I).

See also Figure S3.

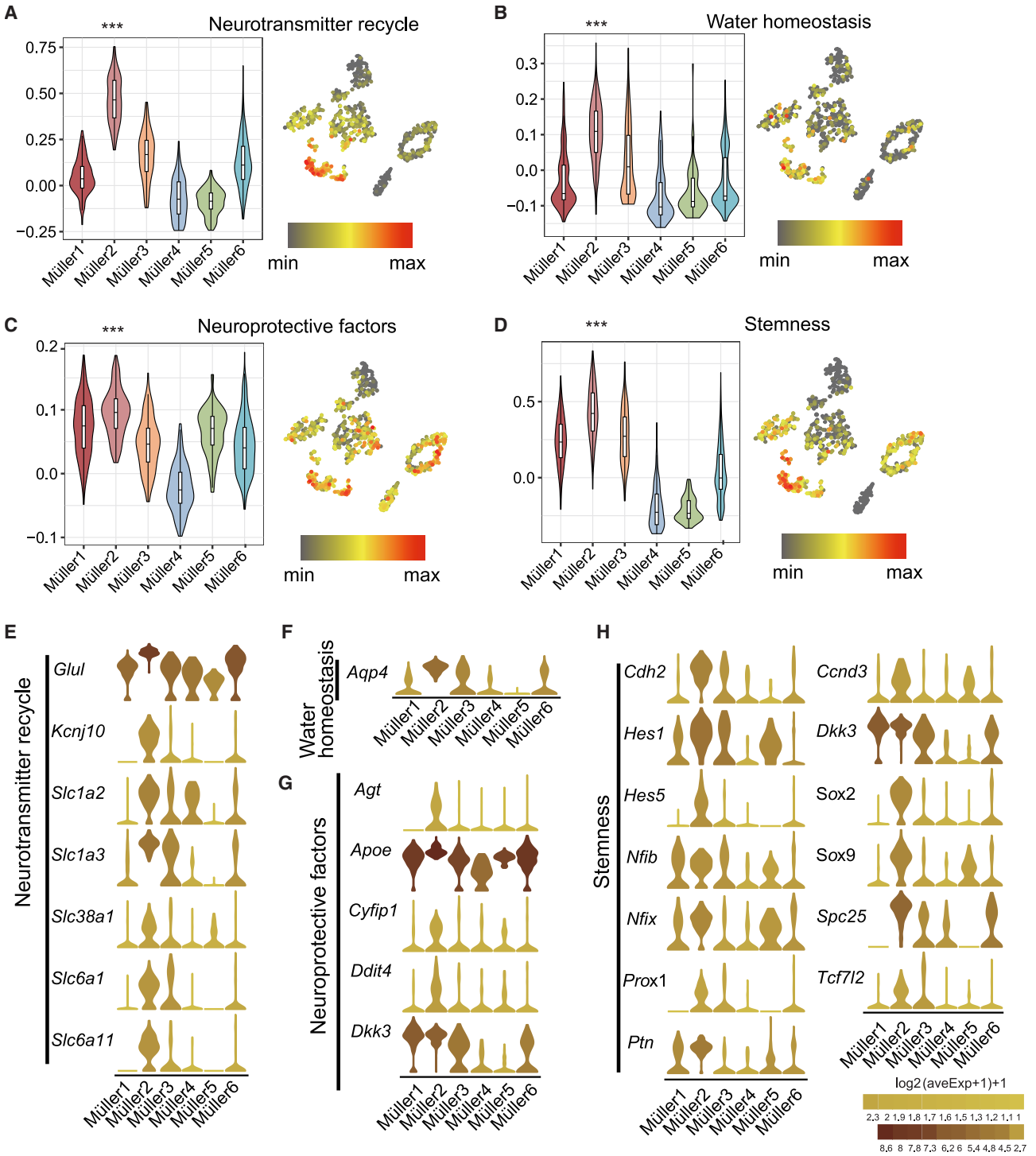

Figure 4. Müller 2 cells are featured with retinal homeostasis and neuroprotection

(A–D) The left violin plot shows that Müller 2 has a higher score in neurotransmitter recycling (A), maintaining water homeostasis (B), excreting neuroprotective factors (C), and stemness (D) than other Müller glia clusters. The boxes show the median (center line) and the quartile range (25%–75%), and the whiskers extend from the quartile to the minimum and maximum values. The t-SNE distribution of four gene signature scores on the right corresponds to the violin plot, and the cluster circled by the dashed line is Müller cluster 2. The statistic result was calculated by Müller cluster 2 and other Müller glia clusters in pairs, and the minimal statistical significance was labeled above the violin plot.

(E–H) The violin plot of high-expression genes in four gene signatures among six Müller glia clusters; genes are colored according to their logarithmic transformation of average expression.

*$p < 0.05$, **$p < 0.01$,***$p < 0.001$, ****$p < 0.0001$, Wilcoxon test. See also Figures S2 and S3.

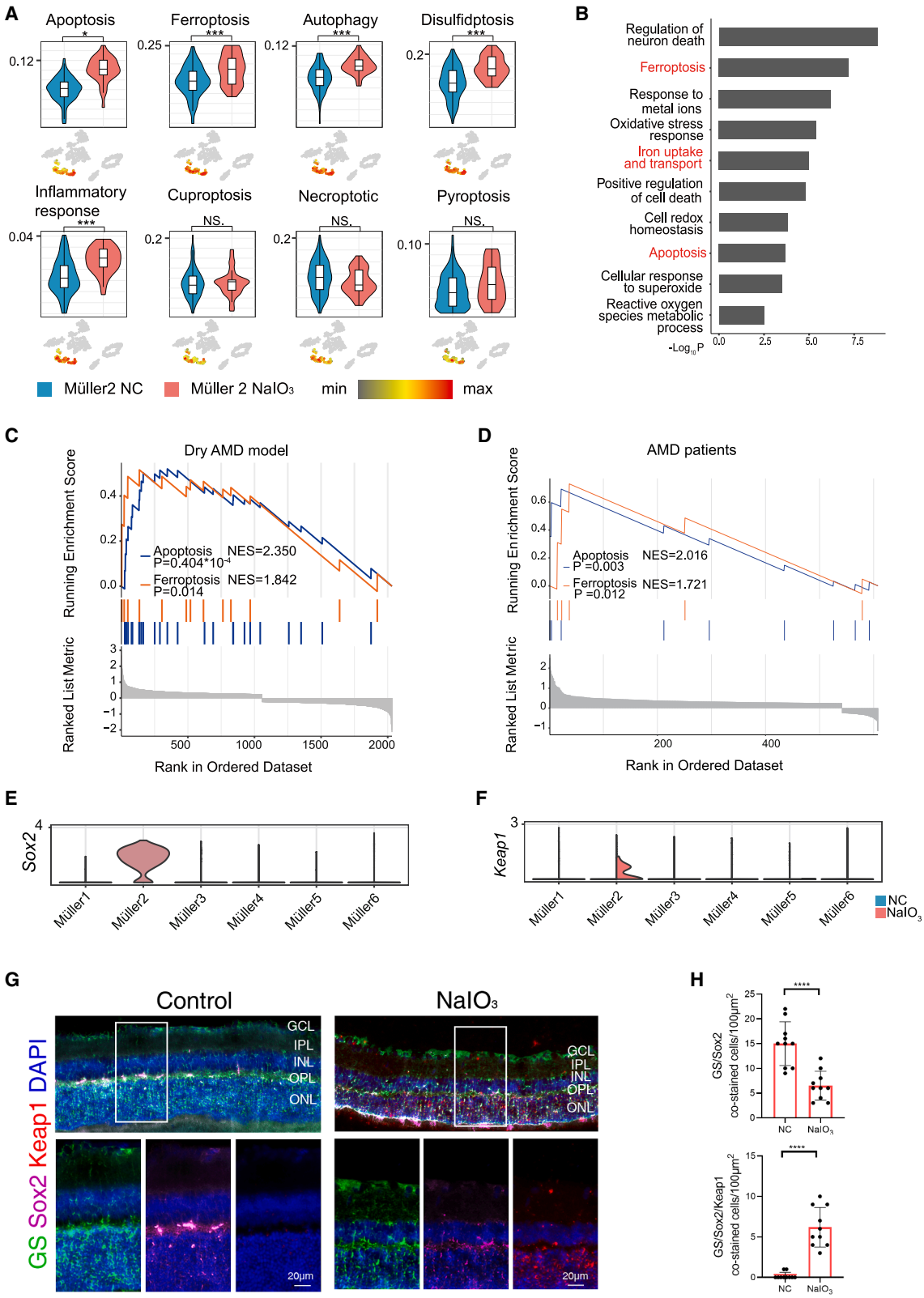

(legend on next page)

potential in our model and the human AMD patient. Importantly, a reduction in the number of this subpopulation may be associated with AMD development. Furthermore, ferroptosis and apoptosis are important causes for the reduction of this cell population. Our study highlights the importance of Müller cells in the progression of AMD. Further research into the mechanism of Müller cell death, such as ferroptosis, will provide a solid foundation for a potential strategy to treat dAMD.

Limitations of the study

There were several limitations in this study. The present result is based on a $NaIO_3$-induced AMD model. The reliability of our results would be increased by using additional models. Thus, we will confirm the data using genetically modified mouse models such as Cryba1$^{fl/fl}$BEST1-cre, CCL2$^{-/-}$, or CCR2$^{-/-}$ in future studies.[63,64] Second, as we have found a similar subpopulation of Müller 2 cells using scRNA-seq data from the AMD patient, it would be more convincing to validate our conclusions in human samples. Third, the Seurat algorithm has been reported to tend to overestimate the number of cell types, especially when the number of cells is large in each cell type.[65] Although the total number of Müller cells is relatively small, it is possible that the number of Müller cell subpopulations is overestimated in our research. Given the heterogeneity of Müller cells, in addition to exploring the protective Müller cell subpopulation, investigating other subsets can also help to improve our understanding of the role of Müller cells in the development of AMD, as well as identifying more potential targets for the treatment of AMD.

RESOURCE AVAILABILITY

Lead contact

Requests for further information and resources should be directed to and will be fulfilled by the lead contact, Bo Qin (qinbozf@163.com).

Materials availability

This study did not generate new unique reagents.

Data and code availability

All of the raw data are available through the Sequence Read Archive (SRA) : (PRJNA1032747). R scripts of this study are available from the lead contact upon reasonable request.

ACKNOWLEDGMENTS

The work was supported by the Natural Science Foundation of Guangdong Province, China (2024A1515012870); Shenzhen Medical Research Funding (A2303042); Shenzhen Science and Technology Innovation Committee, China (JCYJ20230807143413027, JCYJ20220530164600002, and JCYJ20220530164601003); Hunan Provincial Natural Science Foundation of China (2023JJ70007, 2023JJ70039, 2023JJ40001, and 2024JJ9007); Scientific Research Program of Xiangjiang Philanthropy Foundation; Science Research Grant of Aier Eye Hospital Group (AF2201D07 and AF2201D06); Clinic Research Foundation of Aier Eye Hospital Group (grant no. AMF2301D42); and Innovation Capacity Building Project, National Engineering Research Center of Foundational Technologies for CGT Industry, Shenzhen, China, NDRC-High-Technology (2023) no. 447.

AUTHOR CONTRIBUTIONS

B.Z. and D. Liu conceived and designed the study. B.Z. performed all data analyses and generated the figures. C. Zhang, D. Li, Z.L., and J.H. constructed the animal models. Y.L., H.L., M.L., and T.Y. performed experiments on ERG recording, H&E staining, and immunofluorescence. B.Z., D. Liu, and C. Zou prepared the manuscript. B.Q. and C. Zou supervised the work.

DECLARATION OF INTERESTS

The authors declare no competing interests.

STAR★METHODS

Detailed methods are provided in the online version of this paper and include the following:

- KEY RESOURCES TABLE
- EXPERIMENTAL MODEL AND STUDY PARTICIPANT DETAILS
  - Establishment of the $NaIO_3$-induced AMD mouse model
- METHOD DETAILS
  - Preparation of a single-cell suspension of mouse retinas and choroids
  - ScRNA-seq data alignment, processing, and sample aggregation
  - Dimensionality reduction and clustering analysis
  - Reclustering of Müller glia
  - Differential expression analysis
  - Bioinformatics analysis of human AMD ScRNA data
  - Gene functional annotation
  - Cell-type-specific enrichment of genes associated with AMD
  - Pseudotime analysis
  - Scoring of biological processes and gene signatures

Figure 5. Ferroptosis and apoptosis are potential mechanisms that can lead to damage in Müller 2 cells

(A) The violin plots show the apoptosis score, ferroptosis score, autophagy score, disulfidptosis score, inflammatory score, cuproptosis score, necroptotic score, and pyroptosis score in Müller2 between NC (blue) and SI ($NaIO_3$, red) groups, and the lines in the boxplot represent the median values of each cluster. The t-SNEs show the distribution and the expression of score related to eight pathways, and the dots colored with gray are non-Müller2 cells. *$p < 0.05$, **$p < 0.01$, ***$p < 0.001$, ****$p < 0.0001$, Wilcoxon test.

(B) GO and pathway enrichment analysis of the upregulated DEGs in Müller2 cells in the $NaIO_3$ group. p value was derived by a hypergeometric test.

(C) The GSEA analysis shows ferroptosis (orange) and apoptosis (blue) were enriched in Müller2 cells in the $NaIO_3$-treated group.

(D) The GSEA analysis shows ferroptosis (orange) and apoptosis (blue) were enriched in the AMD group of human Müller 4 cluster.

(E) The violin plot of markers in Müller 2 cells.

(F) The violin plot of markers in Müller 2 cells from the SI ($NaIO_3$) group. The square colored blue indicates NC group, and the square colored red indicates SI ($NaIO_3$) group.

(G) Immunofluorescence labeling for glutamine synthetase (GS, green), Sox2 (purple), Keap1 (red), and DAP1 nuclear staining (blue) in the mice retinas. The four graphs on the left represent the control group, while the four graphs on the right represent the $NaIO_3$ group. The graph in the white rectangle is the merge of GS staining, Sox2 staining, and Keap1 staining. Scale bars, 20 μm. GCL, ganglion cell layer; IPL, inner plexiform layer; INL, inner nuclear layer; OPL, outer plexiform layer; ONL, outer nuclear layer.

(H) The quantification of GS$^+$ Sox2$^+$ cells (upper panel) and GS$^+$ Sox2$^+$ Keap1$^+$ cells (lower panel) was performed by counting the number of co-stained cells per square 100 μm in 10 fields of the sections from three mice in each group (at least 5 sections coming from 2 to 3 different animals). Error bars represented SD (p values reflected comparison to the control samples). ****$p < 0.001$, t test. See also Figures S4 and S5.

- Immunofluorescence staining
- QUANTIFICATION AND STATISTICAL ANALYSIS
  - Statistical analysis

SUPPLEMENTAL INFORMATION

Supplemental information can be found online at https://doi.org/10.1016/j.isci.2025.112464.

Received: August 5, 2024
Revised: December 21, 2024
Accepted: April 14, 2025
Published: April 17, 2025

REFERENCES

1. Rim, T.H., Kawasaki, R., Tham, Y.-C., Kang, S.W., Ruamviboonsuk, P., Bikbov, M.M., Miyake, M., Hao, J., Fletcher, A., Sasaki, M., et al. (2020). Prevalence and Pattern of Geographic Atrophy in Asia: The Asian Eye Epidemiology Consortium. Ophthalmology *127*, 1371–1381. https://doi.org/10.1016/j.ophtha.2020.04.019.
2. Zeng, B., Liu, D.C., Huang, J.G., Xia, X.B., and Qin, B. (2024). PdmIRD: missense variants pathogenicity prediction for inherited retinal diseases in a disease-specific manner. Hum. Genet. *143*, 331–342. https://doi.org/10.1007/s00439-024-02645-6.
3. Fleckenstein, M., Keenan, T.D.L., Guymer, R.H., Chakravarthy, U., Schmitz-Valckenberg, S., Klaver, C.C., Wong, W.T., and Chew, E.Y. (2021). Age-related macular degeneration. Nat. Rev. Dis. Primers *7*, 31. https://doi.org/10.1038/s41572-021-00265-2.
4. Tan, Y., Huang, J., Li, D., Zou, C., Liu, D., and Qin, B. (2023). Single-cell RNA sequencing in dissecting microenvironment of age-related macular degeneration: Challenges and perspectives. Ageing Res. Rev. *90*, 102030. https://doi.org/10.1016/j.arr.2023.102030.
5. Zauhar, R., Biber, J., Jabri, Y., Kim, M., Hu, J., Kaplan, L., Pfaller, A.M., Schäfer, N., Enzmann, V., Schlötzer-Schrehardt, U., et al. (2022). As in Real Estate, Location Matters: Cellular Expression of Complement Varies Between Macular and Peripheral Regions of the Retina and Supporting Tissues. Front. Immunol. *13*, 895519. https://doi.org/10.3389/fimmu.2022.895519.
6. Collin, J., Hasoon, M.S.R., Zerti, D., Hammadi, S., Dorgau, B., Clarke, L., Steel, D., Hussain, R., Coxhead, J., Lisgo, S., et al. (2023). Single cell RNA sequencing reveals transcriptional changes of human choroidal and retinal pigment epithelium cells during fetal development, in healthy adult and intermediate age-related macular degeneration. Hum. Mol. Genet. *32*, 1698–1710. https://doi.org/10.1093/hmg/ddad007.
7. Kuchroo, M., Distasio, M., Song, E., Calapkulu, E., Zhang, L., Ige, M., Sheth, A.H., Majdoubi, A., Menon, M., Tong, A., et al. (2023). Single-cell analysis reveals inflammatory interactions driving macular degeneration. Nat. Commun. *14*, 2589–2622. https://doi.org/10.1038/s41467-023-37025-7.
8. Coughlin, B.A., Feenstra, D.J., and Mohr, S. (2017). Müller Cells and Diabetic Retinopathy. Vis. Res. *139*, 93–100. https://doi.org/10.1016/j.visres.2017.03.013.
9. Wang, M., Wang, X., Zhao, L., Ma, W., Rodriguez, I.R., Fariss, R.N., and Wong, W.T. (2014). Macroglia-microglia interactions via TSPO signaling regulates microglial activation in the mouse retina. J. Neurosci. *34*, 3793–3806. https://doi.org/10.1523/JNEUROSCI.3153-13.2014.
10. Liu, Y., Li, L., Pan, N., Gu, J., Qiu, Z., Cao, G., Dou, Y., Dong, L., Shuai, J., and Sang, A. (2021). TNF-α released from retinal Müller cells aggravates retinal pigment epithelium cell apoptosis by upregulating mitophagy during diabetic retinopathy. Biochem. Biophys. Res. Commun. *561*, 143–150. https://doi.org/10.1016/j.bbrc.2021.05.027.
11. Hu, X., Zhao, G.L., Xu, M.X., Zhou, H., Li, F., Miao, Y., Lei, B., Yang, X.L., and Wang, Z. (2021). Interplay between Müller cells and microglia aggravates retinal inflammatory response in experimental glaucoma. J. Neuroinflammation *18*, 303–319. https://doi.org/10.1186/s12974-021-02366-x.
12. Velez, G., Weingarden, A.R., Tucker, B.A., Lei, H., Kazlauskas, A., and Young, M.J. (2012). Retinal pigment epithelium and müller progenitor cell interaction increase müller progenitor cell expression of PDGFRα and ability to induce proliferative vitreoretinopathy in a rabbit model. Stem Cells Int. *2012*, 106486. https://doi.org/10.1155/2012/106486.
13. Liu, B., He, J., Zhong, L., Huang, L., Gong, B., Hu, J., Qian, H., and Yang, Z. (2022). Single-cell transcriptome reveals diversity of Müller cells with different metabolic-mitochondrial signatures in normal and degenerated macula. Front. Neurosci. *16*, 1079498–1079510. https://doi.org/10.3389/fnins.2022.1079498.
14. Aredo, B., Kumar, A., Chen, B., Xing, C., and Ufret-Vincenty, R.L. (2023). Single Cell RNA Sequencing Analysis of Mouse Retina Identifies a Subpopulation of Muller Glia Involved in Retinal Recovery From Injury in the FCD-LIRD Model. Investig. Ophthalmol. Vis. Sci. *64*, 2–4. https://doi.org/10.1167/iovs.64.11.2.
15. Henning, Y., Blind, U.S., Larafa, S., Matschke, J., and Fandrey, J. (2022). Hypoxia aggravates ferroptosis in RPE cells by promoting the Fenton reaction. Cell Death Dis. *13*, 662. https://doi.org/10.1038/s41419-022-05121-z.
16. Wang, J., Iacovelli, J., Spencer, C., and Saint-Geniez, M. (2014). Direct effect of sodium iodate on neurosensory retina. Investig. Ophthalmol. Vis. Sci. *55*, 1941–1953. https://doi.org/10.1167/iovs.13-13075.
17. Tong, Y., Wu, Y., Ma, J., Ikeda, M., Ide, T., Griffin, C.T., Ding, X.Q., and Wang, S. (2023). Comparative mechanistic study of RPE cell death induced by different oxidative stresses. Redox Biol. *65*, 102840. https://doi.org/10.1016/j.redox.2023.102840.
18. Su, W., Gao, Y., Jia, X., Chen, X., Wu, J., Wen, Y., Shi, Y., Zhu, Y., and Zhuo, Y. (2023). Single-cell transcriptome atlas of spontaneous dry age-related macular degeneration in macaques. Fundam. Res. *8*, nwaa179. https://doi.org/10.1016/j.fmre.2023.02.028.
19. Navneet, S., Wilson, K., and Rohrer, B. (2024). Müller Glial Cells in the Macula: Their Activation and Cell-Cell Interactions in Age-Related Macular Degeneration. Investig. Ophthalmol. Vis. Sci. *65*, 42. https://doi.org/10.1167/iovs.65.2.42.
20. Enzbrenner, A., Zulliger, R., Biber, J., Pousa, A.M.Q., Schäfer, N., Stucki, C., Giroud, N., Berrera, M., Kortvely, E., Schmucki, R., et al. (2021). Sodium iodate-induced degeneration results in local complement changes and inflammatory processes in murine retina. Int. J. Mol. Sci. *22*, 9218–9316. https://doi.org/10.3390/ijms22179218.
21. Tang, P.H., Kono, M., Koutalos, Y., Ablonczy, Z., and Crouch, R.K. (2013). New insights into retinoid metabolism and cycling within the retina. Prog. Retin. Eye Res. *32*, 148–163. https://doi.org/10.1016/j.preteyeres.2012.09.002.
22. Fadl, B.R., Brodie, S.A., Malasky, M., Boland, J.F., Kelly, M.C., Kelley, M.W., Boger, E., Fariss, R., Swaroop, A., and Campello, L. (2020). An optimized protocol for retina single-cell rna sequencing. Mol. Vis. *26*, 705–717. https://doi.org/10.37628/molvis.2020.26.705.
23. Cowan, C.S., Renner, M., De Gennaro, M., Gross-Scherf, B., Goldblum, D., Hou, Y., Munz, M., Rodrigues, T.M., Krol, J., Szikra, T., et al. (2020). Cell Types of the Human Retina and Its Organoids at Single-Cell Resolution. Cell *182*, 1623–1640.e34. https://doi.org/10.1016/j.cell.2020.08.013.
24. Kunze, V.P., Angueyra, J.M., Ball, J.M., Thomsen, M.B., Li, X., Sabnis, A., Nadal-Nicolás, F.M., and Li, W. (2024). Neurexin 3 is required for the specific S-cone to S-cone bipolar cell synapse in the mammalian retina. Preprint at bioRxiv. https://doi.org/10.1101/2023.02.13.527055.
25. Deng, Y., Bao, F., Dai, Q., Wu, L.F., and Altschuler, S.J. (2015). Scalable analysis of cell type composition from single-cell transcriptomics using deep recurrent learning. Cancer Cell *2*, 1–17. https://doi.org/10.1038/s41592-019-0353-7.Scalable.

26. Chen, Y., Dong, Y., Yan, J., Wang, L., Yu, S., Jiao, K., and Paquet-Durand, F. (2022). Single-Cell Transcriptomic Profiling in Inherited Retinal Degeneration Reveals Distinct Metabolic Pathways in Rod and Cone Photoreceptors. Int. J. Mol. Sci. *23*, 12170. https://doi.org/10.3390/ijms232012170.

27. Voigt, A.P., Mulfaul, K., Mullin, N.K., Flamme-Wiese, M.J., Giacalone, J.C., Stone, E.M., Tucker, B.A., Scheetz, T.E., and Mullins, R.F. (2019). Single-cell transcriptomics of the human retinal pigment epithelium and choroid in health and macular degeneration. Proc. Natl. Acad. Sci. USA *116*, 24100–24107. https://doi.org/10.1073/pnas.1914143116.

28. Rheaume, B.A., Jereen, A., Bolisetty, M., Sajid, M.S., Yang, Y., Renna, K., Sun, L., Robson, P., and Trakhtenberg, E.F. (2018). Single cell transcriptome profiling of retinal ganglion cells identifies cellular subtypes. Nat. Commun. *9*, 2759. https://doi.org/10.1038/s41467-018-05134-3.

29. Lehmann, G.L., Hanke-Gogokhia, C., Hu, Y., Bareja, R., Salfati, Z., Ginsberg, M., Nolan, D.J., Mendez-Huergo, S.P., Dalotto-Moreno, T., Wojcinski, A., et al. (2020). Single-cell profiling reveals an endothelium-mediated immunomodulatory pathway in the eye choroid. J. Exp. Med. *217*, e20190730. https://doi.org/10.1084/jem.20190730.

30. Fritsche, L.G., Igl, W., Bailey, J.N.C., Grassmann, F., Sengupta, S., Gorski, M., Bragg-Gresham, J.L., Burdon, K.P., Hebbring, S.J., Wen, C., et al. (2016). A large genome-wide association study of age-related macular degeneration highlights contributions of rare and common variants. Nat. Genet. *48*, 134–143. https://doi.org/10.1038/ng.3448.

31. Menon, M., Mohammadi, S., Davila-Velderrain, J., Goods, B.A., Cadwell, T.D., Xing, Y., Stemmer-Rachamimov, A., Shalek, A.K., Love, J.C., Kellis, M., and Hafler, B.P. (2019). Single-cell transcriptomic atlas of the human retina identifies cell types associated with age-related macular degeneration. Nat. Commun. *10*, 4902. https://doi.org/10.1038/s41467-019-12780-8.

32. Eastlake, K., Lamb, W.D.B., Luis, J., Khaw, P.T., Jayaram, H., and Limb, G.A. (2021). Prospects for the application of Müller glia and their derivatives in retinal regenerative therapies. Prog. Retin. Eye Res. *85*, 100970. https://doi.org/10.1016/j.preteyeres.2021.100970.

33. Ashburner, M., Ball, C.A., Blake, J.A., Botstein, D., Butler, H., Cherry, J.M., Davis, A.P., Dolinski, K., Dwight, S.S., Eppig, J.T., et al. (2000). Gene Ontology: tool for the unification of biology. Nat. Genet. *25*, 25–29. https://doi.org/10.1038/75556.

34. Bringmann, A., Pannicke, T., Grosche, J., Francke, M., Wiedemann, P., Skatchkov, S.N., Osborne, N.N., and Reichenbach, A. (2006). Müller cells in the healthy and diseased retina. Prog. Retin. Eye Res. *25*, 397–424. https://doi.org/10.1016/j.preteyeres.2006.05.003.

35. Bringmann, A., Iandiev, I., Pannicke, T., Wurm, A., Hollborn, M., Wiedemann, P., Osborne, N.N., and Reichenbach, A. (2009). Cellular signaling and factors involved in Müller cell gliosis: Neuroprotective and detrimental effects. Prog. Retin. Eye Res. *28*, 423–451. https://doi.org/10.1016/j.preteyeres.2009.07.001.

36. Couturier, A., Blot, G., Vignaud, L., Nanteau, C., Slembrouck-Brec, A., Fradot, V., Acar, N., Sahel, J.A., Tadayoni, R., Thuret, G., et al. (2021). Reproducing diabetic retinopathy features using newly developed human induced-pluripotent stem cell-derived retinal Müller glial cells. Glia *69*, 1679–1693. https://doi.org/10.1002/glia.23983.

37. Boisvert, M.M., Erikson, G.A., Shokhirev, M.N., and Allen, N.J. (2018). The Aging Astrocyte Transcriptome from Multiple Regions of the Mouse Brain. Cell Rep. *22*, 269–285. https://doi.org/10.1016/j.celrep.2017.12.039.

38. Campbell, W.A., El-Hodiri, H.M., Torres, D., Hawthorn, E.C., Kelly, L.E., Volkov, L., Akanonu, D., and Fischer, A.J. (2023). Chromatin access regulates the formation of Müller glia-derived progenitor cells in the retina. Glia *71*, 1729–1754. https://doi.org/10.1002/glia.24366.

39. Koppula, P., Lei, G., Zhang, Y., Yan, Y., Mao, C., Kondiparthi, L., Shi, J., Liu, X., Horbath, A., Das, M., et al. (2022). A targetable CoQ-FSP1 axis drives ferroptosis- and radiation-resistance in KEAP1 inactive lung cancers. Nat. Commun. *13*, 2206. https://doi.org/10.1038/s41467-022-29905-1.

40. Palko, S.I., Saba, N.J., Mullane, E., Nicholas, B.D., Nagasaka, Y., Ambati, J., Gelfand, B.D., Ishigami, A., Bargagna-Mohan, P., and Mohan, R. (2022). Compartmentalized citrullination in Muller glial endfeet during retinal degeneration. Proc. Natl. Acad. Sci. USA *119*, e2121875125. https://doi.org/10.1073/pnas.2121875119.

41. Powner, M.B., Gillies, M.C., Zhu, M., Vevis, K., Hunyor, A.P., and Fruttiger, M. (2013). Loss of Müller's cells and photoreceptors in macular telangiectasia type 2. Ophthalmology *120*, 2344–2352. https://doi.org/10.1016/j.ophtha.2013.04.013.

42. Carpi-Santos, R., de Melo Reis, R.A., Gomes, F.C.A., and Calaza, K.C. (2022). Contribution of Müller Cells in the Diabetic Retinopathy Development: Focus on Oxidative Stress and Inflammation. Antioxidants *11*, 617–629. https://doi.org/10.3390/antiox11040617.

43. Wang, J.H., Wong, R.C.B., and Liu, G.S. (2023). Retinal Aging Transcriptome and Cellular Landscape in Association With the Progression of Age-Related Macular Degeneration. Investig. Ophthalmol. Vis. Sci. *64*, 32. https://doi.org/10.1167/iovs.64.4.32.

44. Graca, A.B., Hippert, C., and Pearson, R.A. (2018). Müller glia reactivity and development of gliosis in response to pathological conditions. Adv. Exp. Med. Biol. *1074*, 303–308. https://doi.org/10.1007/978-3-319-75402-4_37.

45. Martins, R.R., Zamzam, M., Tracey-White, D., Moosajee, M., Thummel, R., Henriques, C.M., and MacDonald, R.B. (2022). Müller Glia maintain their regenerative potential despite degeneration in the aged zebrafish retina. Aging Cell *21*, 135977–e13620. https://doi.org/10.1111/acel.13597.

46. Calì, T., Ottolini, D., and Brini, M. (2013). Calcium and endoplasmic reticulum-mitochondria tethering in neurodegeneration. DNA Cell Biol. *32*, 140–146. https://doi.org/10.1089/dna.2013.2011.

47. Bringmann, A., and Wiedemann, P. (2012). Müller glial cells in retinal disease. Ophthalmologica *227*, 1–19. https://doi.org/10.1159/000328979.

48. Goldman, D. (2014). Müller glial cell reprogramming and retina regeneration. Nat. Rev. Neurosci. *15*, 431–442. https://doi.org/10.1038/nrn3723.

49. Agarwal, D., Do, H., Mazo, K.W., Chopra, M., and Wahlin, K.J. (2023). Restoring vision and rebuilding the retina by Müller glial cell reprogramming. Stem Cell Res. *66*, 103006. https://doi.org/10.1016/j.scr.2022.103006.

50. Chen, H., Ji, Y., Yan, X., Su, G., Chen, L., and Xiao, J. (2018). Berberine attenuates apoptosis in rat retinal Müller cells stimulated with high glucose via enhancing autophagy and the AMPK/mTOR signaling. Biomed. Pharmacother. *108*, 1201–1207. https://doi.org/10.1016/j.biopha.2018.09.140.

51. Wu, M., Yang, S., Elliott, M.H., Fu, D., Wilson, K., Zhang, J., Du, M., Chen, J., and Lyons, T. (2012). Oxidative and endoplasmic reticulum stresses mediate apoptosis induced by modified LDL in human retinal Müller cells. Investig. Ophthalmol. Vis. Sci. *53*, 4595–4604. https://doi.org/10.1167/iovs.12-9910.

52. Fietz, A., Hurst, J., and Schnichels, S. (2022). Out of the Shadow: Blue Light Exposure Induces Apoptosis in Müller Cells. Int. J. Mol. Sci. *23*, 14540. https://doi.org/10.3390/ijms232314540.

53. Somasundaran, S., Constable, I.J., Mellough, C.B., and Carvalho, L.S. (2020). Retinal pigment epithelium and age-related macular degeneration: A review of major disease mechanisms. Clin. Exp. Ophthalmol. *48*, 1043–1056. https://doi.org/10.1111/ceo.13834.

54. Dunaief, J.L., Dentchev, T., Ying, G.S., and Milam, A.H. (2002). The role of apoptosis in age-related macular degeneration. Arch. Ophthalmol. *120*, 1435–1442. https://doi.org/10.1001/archopht.120.11.1435.

55. Liu, B., Wang, W., Shah, A., Yu, M., Liu, Y., He, L., Dang, J., Yang, L., Yan, M., Ying, Y., et al. (2021). Sodium iodate induces ferroptosis in human retinal pigment epithelium ARPE-19 cells. Cell Death Dis. *12*, 230. https://doi.org/10.1038/s41419-021-03520-2.

56. Yao, F., Peng, J., Zhang, E., Ji, D., Gao, Z., Tang, Y., Yao, X., and Xia, X. (2023). Pathologically high intraocular pressure disturbs normal iron

homeostasis and leads to retinal ganglion cell ferroptosis in glaucoma. Cell Death Differ. *30*, 69–81. https://doi.org/10.1038/s41418-022-01046-4.

57. Li, Y., Wen, Y., Liu, X., Li, Z., Lin, B., Deng, C., Yu, Z., Zhu, Y., Zhao, L., Su, W., and Zhuo, Y. (2022). Single-cell RNA sequencing reveals a landscape and targeted treatment of ferroptosis in retinal ischemia/reperfusion injury. J. Neuroinflammation *19*, 261–320. https://doi.org/10.1186/s12974-022-02621-9.

58. Zhao, T., Guo, X., and Sun, Y. (2021). Iron Accumulation and lipid peroxidation in the aging retina: Implication of ferroptosis in age-related macular degeneration. Aging Dis. *12*, 529–551. https://doi.org/10.14336/AD.2020.0912.

59. Liu, D., Liu, Z., Liao, H., Chen, Z.-S., and Qin, B. (2024). Ferroptosis as a potential therapeutic target for age-related macular degeneration. Drug Discov. Today *29*, 103920. https://doi.org/10.1016/j.drudis.2024.103920.

60. Yang, M., Tsui, M.G., Tsang, J.K.W., Goit, R.K., Yao, K.M., So, K.F., Lam, W.C., and Lo, A.C.Y. (2022). Involvement of FSP1-CoQ10-NADH and GSH-GPx-4 pathways in retinal pigment epithelium ferroptosis. Cell Death Dis. *13*, 468. https://doi.org/10.1038/s41419-022-04924-4.

61. Sun, Y., Zheng, Y., Wang, C., and Liu, Y. (2018). Glutathione depletion induces ferroptosis, autophagy, and premature cell senescence in retinal pigment epithelial cells article. Cell Death Dis. *9*, 753. https://doi.org/10.1038/s41419-018-0794-4.

62. Liu, Z., Huang, J., Li, D., Zhang, C., Wan, H., Zeng, B., Tan, Y., Zhong, F., Liao, H., Liu, M., et al. (2024). Targeting ZIP8 mediated ferroptosis as a novel strategy to protect against the retinal pigment epithelial degeneration. Free Radic. Biol. Med. *214*, 42–53.

63. Valapala, M., Wilson, C., Hose, S., Bhutto, I.A., Grebe, R., Dong, A., Greenbaum, S., Gu, L., Sengupta, S., Cano, M., et al. (2014). Lysosomal-mediated waste clearance in retinal pigment epithelial cells is regulated by CRYBA1/βA3/A1-crystallin via V-ATPase-MTORC1 signaling. Autophagy *10*, 480–496. https://doi.org/10.4161/auto.27292.

64. Ambati, J., Anand, A., Fernandez, S., Sakurai, E., Lynn, B.C., Kuziel, W.A., Rollins, B.J., and Ambati, B.K. (2003). An animal model of age-related macular degeneration in senescent Ccl-2- or Ccr-2-deficient mice. Nat. Med. *9*, 1390–1397. https://doi.org/10.1038/nm950.

65. Yu, L., Cao, Y., Yang, J.Y.H., and Yang, P. (2022). Benchmarking clustering algorithms on estimating the number of cell types from single-cell RNA-sequencing data. Genome Biol. *23*, 49. https://doi.org/10.1186/s13059-022-02622-0.

66. Zheng, G.X.Y., Terry, J.M., Belgrader, P., Ryvkin, P., Bent, Z.W., Wilson, R., Ziraldo, S.B., Wheeler, T.D., McDermott, G.P., Zhu, J., et al. (2017). Massively parallel digital transcriptional profiling of single cells. Nat. Commun. *8*, 14049. https://doi.org/10.1038/ncomms14049.

67. Wingett, S.W., and Andrews, S. (2018). Fastq screen: A tool for multi-genome mapping and quality control. F1000Res. *7*, 1338–1414. https://doi.org/10.12688/f1000research.15931.1.

68. Hao, Y., Hao, S., Andersen-Nissen, E., Mauck, W.M., Zheng, S., Butler, A., Lee, M.J., Wilk, A.J., Darby, C., Zager, M., et al. (2021). Integrated analysis of multimodal single-cell data. Cell *184*, 3573–3587.e29. https://doi.org/10.1016/j.cell.2021.04.048.

69. Yu, G., Wang, L.-G., Han, Y., and He, Q.-Y. (2012). clusterProfiler: an R package for comparing biological themes among gene clusters. OMICS *16*, 284–287. https://doi.org/10.1089/omi.2011.0118.

70. Wickham, H. (2016). ggplot2: Elegant Graphics for Data Analysis (Springer-Verlag New York).

71. Zhou, Y., Zhou, B., Pache, L., Chang, M., Khodabakhshi, A.H., Tanaseichuk, O., Benner, C., and Chanda, S.K. (2019). Metascape provides a biologist-oriented resource for the analysis of systems-level datasets. Nat. Commun. *10*, 1523. https://doi.org/10.1038/s41467-019-09234-6.

72. Yu, G. (2023). enrichplot: Visualization of Functional Enrichment Result, https://doi.org/10.18129/B9.bioc.enrichplot https://doi.org/10.18129/B9.bioc.enrichplot.

73. Mancarci, O. (2019). homologene: Quick Access to Homologene and Gene Annotation Updates.

74. Qiu, X., Mao, Q., Tang, Y., Wang, L., Chawla, R., Pliner, H.A., and Trapnell, C. (2017). Reversed graph embedding resolves complex single-cell trajectories. Nat. Methods *14*, 979–982. https://doi.org/10.1038/nmeth.4402.

75. Sun, L., Wang, R., Hu, G., Liu, H., Lv, K., Duan, Y., Shen, N., Wu, J., Hu, J., Liu, Y., et al. (2021). Single cell RNA sequencing (scRNA-Seq) deciphering pathological alterations in streptozotocin-induced diabetic retinas. Exp. Eye Res. *210*, 108718. https://doi.org/10.1016/j.exer.2021.108718.

76. Kanehisa, M., and Goto, S. (2000). KEGG: Kyoto Encyclopedia of Genes and Genomes. Nucleic Acids Res. *28*, 27–30. https://doi.org/10.3892/ol.2020.11439.

77. Zhou, N., Yuan, X., Du, Q., Zhang, Z., Shi, X., Bao, J., Ning, Y., and Peng, L. (2023). FerrDb V2: update of the manually curated database of ferroptosis regulators and ferroptosis-disease associations. Nucleic Acids Res. *51*, D571–D582. https://doi.org/10.1093/nar/gkac935.

78. Ma, Z., Chen, C., Tang, P., Zhang, H., Yue, J., and Yu, Z. (2017). BNIP3 induces apoptosis and protective autophagy under hypoxia in esophageal squamous cell carcinoma cell lines: BNIP3 regulates cell death. Dis. Esophagus *30*, 1–8. https://doi.org/10.1093/dote/dox059.

79. Verhagen, A.M., Ekert, P.G., Pakusch, M., Silke, J., Connolly, L.M., Reid, G.E., Moritz, R.L., Simpson, R.J., and Vaux, D.L. (2000). Identification of DIABLO, a mammalian protein that promotes apoptosis by binding to and antagonizing IAP proteins. Cell *102*, 43–53. https://doi.org/10.1016/S0092-8674(00)00009-X.

STAR★METHODS

KEY RESOURCES TABLE

REAGENT or RESOURCE	SOURCE	IDENTIFIER
Antibodies		
Glutamine synthetase antibody	ABclonal	Cat. No. A5437
HRP-linked secondary antibody	Abcam	Cat. No. ab7090
SOX2 antibody	Cell Signaling Technology,	Cat. No. 3579
KEAP1 antibody	ABclonal	Cat. No. A25951
Chemicals, peptides, and recombinant proteins		
Alexa FluorTM 488-labeled tyramide	Thermo Fisher Scientific	Cat. No.B40953
Antibody eluent	Absin	Cat.No abs994
Alexa FluorTM 555-labeled tyramide	Thermo Fisher Scientific	Cat. No. B40955
Alexa FluorTM 647-labeled tyramide	Thermo Fisher Scientific	Cat.No. B40958
Sodium iodate	Sigma	71702-25G
DAPI	Sigma	D9542
Critical commercial assays		
Chromium Single Cell 3′ v3.1 Reagent Kit	10× Genomics	Cat# PN-120237
Deposited data		
Raw data	This paper	PRJNA1032747
Raw and analyzed data	Dwight Edward Stambolian (University of Pennsylvania)	GSE203499
Experimental models: Organisms/strains		
Mouse: C57BL/6J	Gempharmatech Co., LTD	N/A
Software and algorithms		
10× Genomics Mouse mm10 v2020-A	10× Genomics	https://cf.10xgenomics.com/supp/cell-exp/refdata-gex-mm10-2020-A.tar.gz
CellRanger v4.0.0	Zheng et al.[66]	https://www.10xgenomics.com
FastQC v0.11.9	Wingett et al.[67]	https://www.bioinformatics.babraham.ac.uk/projects/fastqc/
R v4.2.3	N/A	https://www.r-project.org
Seurat v4.3.0.1	Hao et al.[68]	https://satijalab.org/seurat
clusterProfiler v4.8.3	Yu et al.[69]	https://www.bioconductor.org/packages/release/bioc/html/clusterProfiler.html
ggplot2 v3.4.2	Wickham[70]	https://cran.r-project.org/web/packages/ggplot2/index.html
Metascape	Zhou et al.[71]	www.metascape.org
enrichplot v1.20.3	Yu et al.[72]	https://bioconductor.org/packages/release/bioc/html/enrichplot.html
homologene v1.4.68.19.3.27	Mancarci[73]	https://cran.r-project.org/web/packages/homologene/index.html
Monocle v2.28.0	Qiu et al.[74]	https://bioconductor.org/packages/release/bioc/html/monocle.html
Other		
Illumina NovaSeq 6000	Illumina	N/A

EXPERIMENTAL MODEL AND STUDY PARTICIPANT DETAILS

Establishment of the $NaIO_3$-induced AMD mouse model

As an *in vitro* model of age-related macular degeneration, the $NaIO_3$-induced mouse model was established. 6-week-old C57BL/6J male mice were purchased from the Gempharmatech Co., LTD. Then the optimal dose (50 mg/kg) of $NaIO_3$ solution was injected into

the abdominal cavity of those mice. The control group was injected with the same amount of saline. Two weeks after the $NaIO_3$ was treated, the electrical activity of their retina in response to a light stimulus was recorded by electroretinogram (ERG), and hematoxylin-eosin (HE) staining was observed to ensure that $NaIO_3$-induced AMD mouse models were successfully established. All procedures were approved by the Jinan University Institutional Animal Care and Use Committee.

METHOD DETAILS

Preparation of a single-cell suspension of mouse retinas and choroids

Two weeks after $NaIO_3$ induced, the mice were used to perform scRNA-seq. Three mice were included in each of the $NaIO_3$-induced model and the NC groups. Due to differences in cell dissociation procedures of retinal and choroidal cells, the retina and choroid tissues of each group were collected and isolated separately. The retina (or choroid) tissues from three mice in the same group were combined and subjected to scRNA sequencing. Combining samples can help reduce technical variability between individual mouse samples, leading to more consistent data from a technical perspective. In addition, since cells from the retina and choroid are very fragile, especially in the $NaIO_3$-treated mice, combining tissues is a solution that preserves a sufficient number of cells for sequencing. Cell dissociation procedures were as previously reported.[22] The cell suspension was collected to check the viability by fluorescence-based cell viability assay and flow cytometry with a dye exclusion method. Only cells with viability over 80% were used for scRNA sequencing.

ScRNA-seq data alignment, processing, and sample aggregation

Gel Bead and Multiplex Kit, Chip Kit (10× Genomics), and Chromium Single Cell 3′ Library (10× Genomics, Genomics chromium platform Illumina NovaSeq 6000) were used to convert the harvested single-cell suspensions into barcoded scRNA-seq libraries. Single-cell RNA libraries were made up of the Chromium Single Cell 3′ v3.1 Reagent Kit (120237; 10× Genomics) according to the manufacturer's instructions, and FastQC software was used for quality control of raw data. All sequenced data were preliminarily processed by CellRanger software (version 4.0.0) and generated three types of files: barcodes.tsv.gz, matrix.mtx.gz, and featuress.tsv.gz. These files were read by the "Read10×" function of the Seurat R package (version 4.3.0.1). Subsequent processes, including data filtration, data normalization, dimensionality reduction, cell clustering, and differential gene expression analysis, were also dependent on Seurat. The original number of cells in NC (retina), NC (choroid), $NaIO_3$ (retina), and $NaIO_3$ (choroid) are 5958, 6474, 6064, and 4583, respectively. Cells with less than 200 genes detected and a mitochondrial gene ratio of more than 20% were excluded.[57,75] A total of 20,725 cells of retinas and choroids (NC, 11,155 cells; $NaIO_3$, 9,570 cells) were analyzed after quality control.

Dimensionality reduction and clustering analysis

The function "ScaleData" was used to scale and center the counts. Then, the "NormalizeData" function was used to log-normalize the counts of each cell (1+counts per 10,000). Dimensionality reduction was achieved by the "RunPCA" function. Cells were visualized through two algorithms: UMAP and t-SNE. They were executed by the "RunUMAP" and "RunTSNE" functions of Seurat (version 4.3.0.1). The "FindNeighbors" and "FindClusters" functions were utilized to identify significant clusters at an appropriate resolution. The clusters that had cell numbers less than 50 were removed. The function "FindAllMarkers" was utilized to identify marker genes of significant clusters. The marker genes were selected according to the avg_log2FC (>0.25) and p_val_adj (<0.05).

Reclustering of Müller glia

To identify subtypes or cells in different states within Müller glia, we extract the counts of the Müller glia cluster to reclustering. Then the "SCTransform" function was used to regularize negative binomial regression to normalize UMI count data, and the subsequent processes were performed as we did on the whole dataset.

Differential expression analysis

Differential expression analysis was performed by the Wilcoxon rank-sum test, which wrapped in the "FindMarkers" function to identify DEGs between $NaIO_3$ groups and NC groups of all clusters (p_val_adj <0.05 and |avg_log2FC| > 0.25) with default parameters.[6,14]

Bioinformatics analysis of human AMD ScRNA data

The scRNA-seq data of a 91-year-old dAMD patient and four controls were downloaded from GEO (GSM6173966, GSM6173968, GSM6173982, GSM6173984, GSM6173986, GSM6173988, GSM6173992, GSM6173994, GSM6173974, and GSM6173976), and the data from macula retina and peripheral retina were used analysis together. The clinical information of those samples could be obtained from the URL (https://www.ncbi.nlm.nih.gov/geo/query/acc.cgi?acc=GSM6173976). The quality control of data is based on the parameters – "nFeature_RNA >100 & nFeature_RNA <5000, per.mt < 15 & nCount_RNA <15000". The other procedures in bioinformatic analysis were the same as the process in the mouse model.

Gene functional annotation

GO and GSEA enrichment analysis were performed by using the "enrichGO" and "gseKEGG" functions of clusterProfiler R package (version 4.8.3), respectively. Metascape (www.metascape.org) was used to conduct GO and pathway analysis with the input of up-regulated DEGs.[71] The results were visualized by the ggplot2 R package (version 3.4.2) and the enrichplot R package (version 1.20.3).

Cell-type-specific enrichment of genes associated with AMD

The AMD-associated genes were a gene set that surrounding the 34 AMD locus regions obtained from the GWAS.[30] The genes were transformed from the "hsapiens" version into the "musculus" version by the "human2mouse"function of the homologene R package (version 1.4.68.19.3.27), and 31 mouse genes matched to AMD were obtained. Then, we calculated the cell type-specific enrichment of each AMD-associated gene as previously described.

Pseudotime analysis

Pseudotime analysis was performed with Monocle package (version 2.28.0).[74] The DEGs were selected to define the process, and functions "reduceDimension" and "orderCells" were used to construct the trajectory. Then, the "BEAM" function was used to detect the DEGs along the pseudotime.

Scoring of biological processes and gene signatures

Individual cells were scored by gene signatures representing certain biological functions, which were executed using the "AddModuleScore" function of the Seurat R package (version 4.3.0.1). To explore the function of the Müller glia sub-population, full gene lists with biological functional signatures were obtained from the GO database, Kyoto Encyclopedia of Genes and Genomes (KEGG) database, and classical literature.[33–35,76] To explore the potential death model of cells, more complete gene sets were constructed. Ferroptosis gene signature included the genes in the Ferrdb database (http://www.zhounan.org/ferrdb/current/), GO database, and KEGG database.[77] For apoptosis gene signature, genes in Deathbase (http://deathbase.org/), GO database, and KEGG database were used. The role of genes in ferroptosis and apoptosis gene signatures was determined by retrieving literature.[77–79] The score of human Müller glia with feature genes of Müller cluster 2 is the same as the steps above.

Immunofluorescence staining

For multiplex immunostaining, the Tyramide Signal Amplification system was employed. After blocking endogenous peroxidase in tissue sections with 3% H_2O_2 for 10 min at room temperature. Tissue sections were blocked with 5% BSA in PBS. Primary antibody Glutamine synthetase (GS) (diluted at 1:100, Abclonal, Cat. No. A5437) was incubated on the sections for overnight at 4°C. The sections were then stained with Alexa FluorTM 488-labeled tyramide (Thermo Fisher Scientific, Cat. No. B40953) and treated with HRP-linked secondary antibody (Abcam, cat. no. ab7090). To release the antibodies, the sections were treated with Antibody eluent (Absin, Cat.No abs994) to remove the antibodies. Following a PBS rinse, the sections were incubated with the primary antibody SOX2 (diluted at 1:100, Cell Signaling Technology, Cat. No. 3579), the secondary antibody, and then treated with HRP-linked Alexa FluorTM 555-labeled tyramide (Thermo Fisher Scientific, Cat. No. B40955). Following the second heating and washing cycle as mentioned above, the sections were incubated with primary antibody (KEAP1, diluted at 1:100, Abclonal, Cat. No. A25951), HRP-linked secondary antibody, Alexa FluorTM 647-labeled tyramide (Thermo Fisher Scientific, Cat. No. B40958), and DAPI counterstained.

QUANTIFICATION AND STATISTICAL ANALYSIS

Statistical analysis

Wilcoxon test was used to perform statistical analysis in the bioinformatics part. Data were analyzed statistically using a two-tailed Student's t test for two group comparisons. To assess significance, a value of $p < 0.05$ was considered statistically significant (*$p < 0.05$; **$p < 0.01$; ***$p < 0.001$; ****$p < 0.0001$). The sample sizes and p-values are indicated in the figure legends.